Journal of Materials Chemistry

Dynamic Article Links

Cite this: *J. Mater. Chem.*, 2012, **22**, 9138

www.rsc.org/materials

PAPER

Encapsulation of self-healing materials by coelectrospinning, emulsion electrospinning, solution blowing and intercalation

S. Sinha-Ray,[a] D. D. Pelot,[a] Z. P. Zhou,[b] A. Rahman,[b] X.-F. Wu[b] and A. L. Yarin*[ac]

Received 6th November 2011, Accepted 2nd March 2012
DOI: 10.1039/c2jm15696b

Different techniques for encapsulating self-healing materials (liquid monomers) inside polymer fibers [polyacrylonitrile (PAN)] and amorphous turbostratic carbon nanotubes (CNTs) were explored. Two types of healing materials were used: dicyclopentadiene (DCPD) and isophorone diisocyanate. To encapsulate the self-healing materials inside polymer nanofibers, coelectrospinning, emulsion electrospinning and emulsion solution blowing were used. The presence of self-healing materials inside polymer fibers was corroborated by using optical and scanning electron microscopy, energy dispersive X-ray spectroscopy, and preferential imprinting of fluorescent dyes. Furthermore, fiber crush tests were used to validate the encapsulation of liquid self-healing agents. Proof-of-concept carbon-fiber–epoxy composites reinforced with ultrathin nanofibrous interlayers of the self-healing core–shell nanofibers were fabricated and the release of self-healing agents in the polymeric matrix was characterized. Consequently, the liquid monomers used for self-healing agents were also intercalated into CNTs using the self-sustained diffusion technique. The intercalated CNTs were studied using transmission electron microscopy, which proved the presence of self-healing materials inside the CNTs.

1. Introduction

Advanced composites made of a polymer matrix (typically thermosetting epoxy) reinforced with high-performance fibers have found rapidly expanding applications in aerospace, aeronautical and ground vehicles, windmill blades, and sports utilities, among others. This is due to their high specific strength and stiffness, excellent manufacturability, superior corrosion resistance and their ability to be tailored for specific properties. Yet, the unique hierarchical fiber architecture embedded in a brittle polymer matrix results in unavoidable crack nucleation and growth in polymer composites when subjected to external loads. From the physical point of view, all the damage and failure processes identified in conventional polymer composites are thermodynamically irreversible, *i.e.* the material properties always gradually degrade with time. Thus, damage monitoring, healing and maintenance costs become high priorities once damage and failure occur in high-value composite structures, especially in military aircraft and spacecraft, as well as antennas on satellites or space stations. Therefore, producing polymer composites carrying self-healing functionality, which mimic biological processes in nature, is highly desirable in materials science and engineering.

In principle, healing micro-cracks *in situ* can significantly increase structural lifetime and suppress maintenance costs of polymer composites. Any crack formation can compromise the material strength, safety and reliability. Hence, it is especially important to avoid micro-cracking in applications where identification is difficult or impossible. To date, the market of composite materials has been continually growing and healable materials are necessary for the continuation of that growth. One of the first attempts to heal a thermoplastic polymeric material was associated with the conventional heating method.[1] In this method, the broken polymer parts are subjected to hot plate welding in which they are elevated to temperatures above their glass transition temperatures. However, it was found that the fractured part always remained the weakest portion.[2]

Historically, engineering has always found inspiration in nature. For example, the ability of mammals to heal themselves autonomously (such as bleeding, bruising, and healing of bone fracture) and return to a previous state is a process that scientists are trying to mimic. As in mammals, self-healing materials should have sub-systems in which automatic responses are triggered by minor damage.[3–5] The very first trial to incorporate such smart healing capabilities in engineering was performed by encasing composites with glass capillaries/tubing filled with self-healing agents.[6] However, handling such systems is troublesome. Therefore, the incorporation of healing agents inside the composites becomes imperative.[4,7] As described in ref. 8,

[a]*Department of Mechanical and Industrial Engineering, University of Illinois at Chicago, 842 W. Taylor St, Chicago IL 60607-7022, USA. E-mail: ayarin@uic.edu; Fax: +1 (312) 413-0447; Tel: +1 (312) 996-3472*
[b]*Department of Mechanical Engineering, North Dakota State University, Fargo, ND 58108-6050, USA*
[c]*Center for Smart Interfaces, Technische Universität Darmstadt, Petersenstr. 32, 64287 Darmstadt, Germany*

the works of several authors on poly(dicyclopentadiene) and Grubbs' catalyst opened the way to using them as healing agents because of their excellent chemical stability. After this seminal discovery, however, substitutes were searched for due to the high cost and limited availability of the catalysts. In this search, tungsten hexachloride was found to be a superior substitute due to its wide availability and enhanced melting point.[8] However, some healing materials, such as isophorone diisocyanates, can use the humidity in the surrounding air as a catalyst, therefore, avoiding the need for a second chemical in the material matrix.[8,9]

All the above-mentioned encapsulation processes of self-healing materials involve chemically complex and expensive routes of manufacturing. Moreover, these routes commonly rely on microscopic hollow fibers or spherical capsules with diameters over 100 μm. The direct incorporation of the healing agents *via* these carriers may adversely influence the superior specific properties of fiber-reinforced polymer composites. In fact, reliable interfacial toughening and self-healing strategies are desired for the ultrathin resin-rich interlayers of these polymer composites where localized damage and interlaminar fracture commonly occur under external loading.[10] In the past years, a novel interfacial toughening technique based on entangling small fibers at interfaces (interlayers) has been proposed,[11,12] which is specifically suitable for toughening fiber-reinforced polymer composites. These toughening small fibers can be compliant continuous polymer nanofibers or polymer-derived carbon nanofibers produced by means of the low-cost electrospinning technique.[13–19] Recent accumulating experimental data[20–23] and modeling results[20] have validated this interfacial toughening strategy. Due to its intrinsic low cost in fabrication, low fiber concentration and ease of merging into the conventional composites processing, this interfacial toughening technique would have a promising future in composites engineering and industry. Yet, this interfacial toughening technique does not carry any self-healing function.

Therefore, in this study, we aim to produce novel ultrathin nanofibrous interlayers carrying both interfacial toughening and self-healing functions for use in fiber-reinforced polymer composites. These nanofibrous interlayers consist of electrospun core–shell polymer nanofibers or carbon nanotubes encapsulating healing agents. In particular, we explore several novel techniques to encapsulate the healing agents inside ultrathin polymer fibers and amorphous turbostratic carbon nanotubes (CNTs), which could add to the structural capabilities of the material. By using coelectrospinning, emulsion electrospinning and emulsion solution blowing, two healing agents were incorporated into the core of micron-size polymer fibers. These three methods offer the capability of encapsulation in a vascular network-like structure. Also, the healing materials were intercalated inside amorphous turbostratic CNTs, which opens up the path for preparing polymer composites with functional characteristics owing to dispersed CNTs along with self-healing capabilities.

To validate the deliverability of healing agent of these core–shell nanofibers and nanotubes, novel fiber-crush tests were designed. Proof-of-concept carbon-fiber–epoxy composites reinforced with the novel nanofibrous self-healing interlayers were fabricated, interlaminar fracture tests were performed, and the toughening and self-healing mechanisms were explored by fractographical analysis of the failure interfaces.

2. Experimental

2.1. Materials

Polyacrylonitrile (PAN, M_w = 150 kDa) was obtained from Polysciences Inc. *N*-dimethyl formamide (DMF) anhydrous 99.8%, dicyclopentadiene (DCPD), isophorone diisocyanate, benzene, Rhodamine B, Grubbs' catalyst and tungsten(VI) chloride were obtained from Sigma Aldrich. Commercial, as-grown, highly graphitic carbon nanotubes (PR-24, Pyrograph III) constitute the CNTs employed in this study. The CNTs contained some iron (<14 000 ppm), and less than 5% moisture, and had inner diameters of 50–100 nm and lengths in the range of 10–100 μm. All the chemicals were used as received without any further purification or change. Copper plates obtained from McMaster-Carr were cut into 1 × 1 in^2 pieces and used as collection plates in the emulsion electrospinning and emulsion solution blowing processes and were further used for the crush tests. The substrates were cleaned with acetone prior to use. Syringe filters of 0.45 μm were obtained from Cole–Parmer.

2.2. Preparation of solutions

For emulsion electrospinning and emulsion solution blowing, emulsions of DCPD in a solution of PAN in DMF and an emulsion of isophorone diisocyanate in a solution of PAN in DMF were prepared using the following route. A 12 wt% PAN solution in DMF was prepared first. Then, DCPD and DMF were added to achieve the concentrations of 8 wt% PAN and 5 wt% DCPD in DMF. For preparing an emulsion containing 8 wt% PAN and 5 wt% isophorone diisocyanate in DMF, all three components were mixed simultaneously. Both solutions were prepared at a temperature of 75 °C with continuous stirring.

For coelectrospinning, a solution of 10 wt% PAN in DMF was prepared for the outer jet (shell) and a solution of 10 wt% DCPD in DMF was prepared for the inner jet (core).

For the intercalation of DCPD or isophorone diisocyanate into CNTs, the following route was employed: 0.2 g of the solute (DCPD or isophorone diisocyanate) was added to 10 g of benzene and then sonicated for about 30–45 minutes until clear solutions were obtained.

2.3. Emulsion electrospinning and solution blowing

Core–shell fibers were prepared by emulsion electrospinning using the standard electrospinning setup described elsewhere.[18,19,24–30] Randomly oriented fibers were collected on a glass slide and copper plates for 1–3 min. The parameters for electrospinning of different emulsions are summarized in Table 1.

For emulsion solution blowing of core–shell nanofibers the experimental setup[28,29] was employed. In brief, a digital syringe pump supplied the emulsion to the needle exit where it was subjected to a co-axial high velocity (~150 to 200 m s^{-1}) air flow field. The air flow was issued from an annular nozzle concentric to the needle supplying the emulsion. The air flow pulled the emulsion jet causing vigorous bending instability similar to that in electrospinning.[15,26,30] The parameters for emulsion solution blowing of the different emulsions are listed in Table 2.

Table 1 Experimental parameters of emulsion electrospinning of two emulsions: PAN and DCPD in DMF, and PAN and isophorone diisocyanate in DMF

Emulsion	Needle to collector distance (cm)	Voltage (kV)	Flow rate (ml h^{-1})
PAN–DCPD–DMF	7–12	16–18	0.3–0.4
PAN–isophorone diisocyanate–DMF	20	20	0.6–0.7

Table 2 Experimental parameters of emulsion solution blowing of two emulsions, namely PAN and DCPD in DMF, and PAN and isophorone diisocyanate in DMF

Emulsion	Needle to collector distance (cm)	Air pressure (psi)	Flow rate (ml h^{-1})
PAN–DCPD–DMF	30–35	30	6
PAN–isophorone diisocyanate–DMF	30–35	30	6

2.4. Coelectrospinning

In addition, standard coelectrospinning was employed to produce core–shell PAN fibers which encapsulated liquid DCPD. During this process, a lab-made coaxial needle setup[15,18,19,24,25] was utilized for generating the core–shell jet. The inner diameter of the exterior needle was 0.97 mm, while the outer and inner diameters of the interior needle were 0.71 mm and 0.48 mm, respectively. The solution of 10 wt% PAN in DMF was issued as the outer jet (shell) and the solution of 10 wt% DCPD in DMF was issued as the inner jet (core). The flow rates of the outer jet (shell) and the inner jet (core) were controlled by two digital syringe pumps as 1.5 ml h^{-1} and 1.0 ml h^{-1}, respectively. A DC voltage of 18 kV was generated by a high DC voltage power supply (Gamma High Voltage Research, Inc., Ormond Beach, FL) and applied between the coaxial needle and an aluminium plate covered with an aluminium foil (used as fiber collector) at a distance of 25 mm.

2.5. Intercalation

The idea of the method of self-sustained diffusion introduced in ref. 31–33 for intercalating carbon nanotubes at room pressure and temperature is discussed in the following. Empty CNTs are blended with a dilute or semi-dilute solution of a solute to be intercalated (polymers, surfactants, nanoparticles, triglycerides and wax in ref. 31–33 or healing agents such as DCPD and isophorone diisocyanate in the present work). The Fickian diffusion of solute and convection rapidly (on the scale of milliseconds) equilibrate the solute concentration inside CNTs with that in the bulk. At this relatively low solute concentration inside CNTs, the intercalation process would have stopped. However, when the solution with suspended CNTs is left to evaporate (the process which lasts for minutes or even hours), the bulk concentration of solute gradually increases, since solvent is lost. The increased solute concentration in the bulk permanently sustains the Fickian diffusion of the solute into CNTs, which allows intercalating them almost completely, sometimes practically filling the entire CNT bore. This process of the self-sustained diffusion is implemented in the present work as described below.

CNTs in powder form with a mass of 0.018–0.024 g were added to each of the solutions involving DCPD or isophorone diisocyanate in benzene. Then, each solution was sonicated for 30 min and the vials were left inside a chemical hood with the cap open to allow all the benzene to evaporate. The benzene evaporation resulted in the self-sustained diffusion of the solutes (DCPD or isophorone diisocyanate) into the CNTs.[31–33] After the benzene completely evaporated, the solute intercalation into CNTs was over. Then, fresh benzene was added to the vials and sonicated for 3–4 min to clean the outside of the CNTs. After that, the content was filtered immediately to isolate the intercalated CNTs which now have a clean outside surface.

It is emphasized that when fresh benzene was added to fully dissolve and clean the solutes deposited outside CNTs, practically no solute is lost from the inside. Indeed, similarly to ref. 34, the solute from the inside can be dissolved in this added benzene only through an open CNT cross-section normal to its axis. Then, the solute molecules are removed from the dissolution front by the Fickian diffusion. As the dissolution front moves into a CNT, the solute gradient in benzene decreases as the length from the opening increases. As a result, the solute concentration level near the dissolution front is sustained longer, which in turn, decelerates the dissolution process. Therefore, with relatively long solute slugs inside relatively long CNTs, the frontal dissolution of solute from the inside rapidly becomes very slow, whereas the dissolution of the solute layer deposited outside CNTs proceeds at a much faster rate and from a much larger area. As a result, the solute deposited outside CNTs dissolves much faster than the one inside, and the losses of the healing materials from CNTs at the rinsing stage are negligibly small.

2.6. Self-healing composite fabrication and interlaminar fracture tests

In addition, a proof-of-concept self-healing polymer composite was fabricated and utilized to validate the deliverability of self-healing agent in a novel polymer composite system, which consisted of six layers of carbon-fiber fabrics (Fiber Glast, OH) in epoxy resin (volume fraction $\sim$ 40%). The epoxy resin was prepared by mixing Epon 828 epoxide (Shell Chemicals, Inc.) with diethylenetriamine curing agent (Shell Chemicals, Inc.) in the volume fraction 100 : 12. About 1% (by weight) Grubbs' catalyst was further added into the resin mixture before infusion. To form the composite panel, the wetted layup method was first applied, in which a thin layer of core–shell PAN nanofibers containing DCPD (produced by coelectrospinning) was inserted at the interface between the 3rd and 4th layers of carbon-fiber fabrics, and a Teflon film was also inserted to generate an artificial crack for interlaminar fracture. After the wetted layup, the vacuum-assisted resin transfer molding (VARTM) technique was further applied to the wetted composite panel to drive off the air bubbles and homogenize the resin inside the fiber fabrics. After curing at room temperature for 24 h, the composite laminate with an ultrathin nanofibrous self-healing layer at the middle interface was cut into small samples with the dimensions $\sim$20 mm $\times$ 5 mm $\times$ 1.7 mm by using a water-cooled diamond rotary saw. Finally, a sharp wedge was used to open the

self-healing samples along the artificial crack to mimic the mode I interlaminar fracture test. Failed sample surfaces were coated with a thin carbon layer for surface characterization of the core–shell nanofibers and exploring the self-healing mechanisms by using a high-resolution scanning electron microscope.

2.7. Observations

All scanning electron microscopy of core–shell fiber mats was done using a JEOL JSM-6320F microscope with a cold emission source. Prior to SEM observation, the fiber mats were sputter-coated with Pt/Pd to a thickness of 6–8 nm. The transmission electron microscopy was done using a JEOL JEM 3010 TEM microscope. The optical images of emulsion electrospun and emulsion solution blown fibers were captured using an Olympus BX51 microscope in refraction mode. The collected coelectrospun core–shell PAN–DCPD fibers were characterized using a IX 71 Olympus optical microscope with the objective magnification of 40× and a fluorescent microscope.

3. Results and discussion

Prior to emulsion electrospinning or emulsion solution blowing, the emulsions were observed carefully both visually and under the optical microscope. It was found that there was no appreciable color difference between the emulsions containing healing agents and pure PAN solutions used as a matrix, in distinction from the PAN–PMMA [poly(methyl methacrylate)], emulsions described in ref. 27. It should also be mentioned that even after leaving the unstirred emulsions on a shelf for a couple of days, there was no visible phase separation similar to that indicated in ref. 27. For further characterization, the emulsions were spread on a glass slide and observed under an optical microscope (Fig. 1). It was found that the DCPD emulsion in PAN–DMF possessed a few tiny droplets with the diameter of about 5–15 μm (Fig. 1). On the other hand, the emulsion of isophorone diisocyanate in PAN–DMF showed no droplets, which means that all the droplets were under submicron scale. In contrast, the emulsions of PMMA in PAN–DMF possessed large droplets of PMMA (with the diameter of about 100 μm).[27] It is emphasized that the formation of core–shell fibers as described below is an indirect proof of the emulsion nature of isophorone diisocyanate in PAN–DMF solutions.

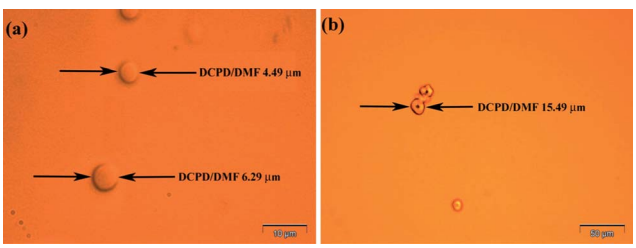

Fig. 1 An emulsion of DCPD–DMF in PAN–DMF. (a) Tiny droplets of DCPD–DMF while the emulsion is wet. (b) Droplets of dried DCPD–DMF embedded in the matrix. It is emphasized that the emulsions are polydisperse, which might explain the fact that droplets in two different samples shown in panels (a) and (b) have different sizes. In addition, it is worth mentioning that droplets flatten when they dry, which can also be responsible for a larger size of the dried droplets in panel (b). The scale bars are 10 μm and 50 μm in (a) and (b), respectively.

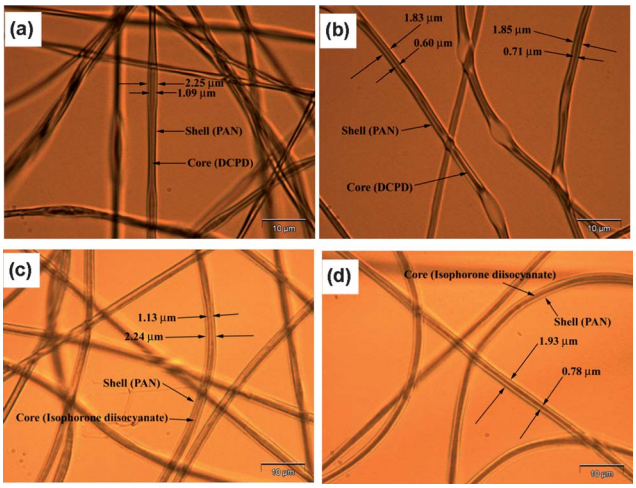

Fig. 2 Optical images of core–shell fibers electrospun from emulsion are shown. Panels (a) and (b) show core–shell fibers obtained from emulsion of DCPD in PAN and DMF, while panels (c) and (d) show core–shell fibers obtained from emulsion of PAN and isophorone diisocyanate in DMF. The scale bar in all images is 10 μm.

The fibers electrospun from emulsions are shown in Fig. 2. The electrospun fibers from an emulsion of 8 wt% PAN and 5 wt% DCPD were collected on a glass slide and observed under an optical microscope in refraction mode (Fig. 2a and b). In all images captured, it was found that the majority of fibers are core–shell fibers. There were very few monolithic fibers. It can be observed that sometimes the fibers are slightly beaded (Fig. 2b), which can be explained by the onset of capillary instability. The diameter of the fiber shell is in an approximate range of 1.5 μm to 3 μm, whereas the core diameter approximate range is from 0.4 μm to 1.5 μm. The emulsion electrospinning of 8 wt% PAN and 5 wt% isophorone diisocyanate in DMF resulted in an abundance of uniform core–shell fibers (Fig. 2c and d). From the optical images it was found that there were no monolithic fibers. In every image inspected, all fibers were core–shell fibers. It was found that the shell diameter in this case ranged from 1.75 μm to 3.81 μm and the core diameter from 0.51 μm to 2.01 μm.

The same emulsions which were used in the emulsion electrospinning were also used in emulsion solution blowing. The solution-blown fibers were collected on glass slides for 1–3 min and inspected under the optical microscope. The optical images of the fibers obtained from the emulsions of PAN–DCPD in DMF and PAN–isophorone diisocyanate in DMF are shown in Fig. 3a, b and c, d, respectively. It can be seen that the majority of the collected fibers reveal the core–shell structure. It can be seen from Fig. 3a and b that for PAN–DCPD in DMF the shell diameter approximately ranges from 1.35 μm to 3.00 μm, while the core diameter is in the range of 0.44 μm to 1.30 μm. For PAN–isophorone diisocyanate in DMF (Fig. 3c and d), the shell diameter ranges from 1.80 μm to 2.90 μm, while the core diameter ranges from 0.40 μm to 0.95 μm.

Fig. 4 shows the coelectrospun core–shell PAN–DCPD nanofibers. It can be observed (Fig. 4a) that the fibers contain about 10 wt% of liquid DCPD dissolved in DMF as the core

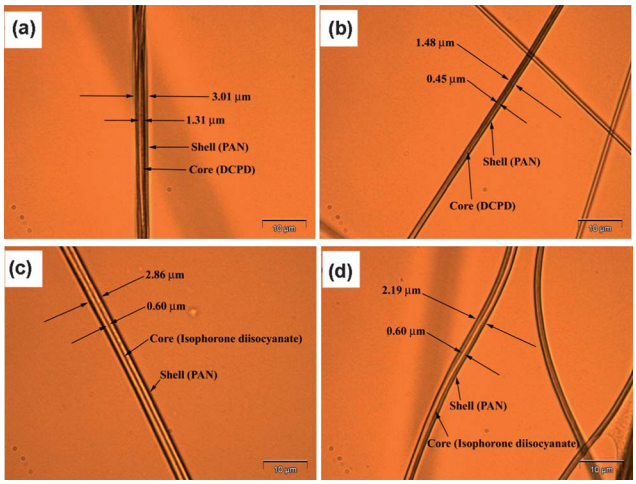

Fig. 3 Optical images of the core–shell fibers obtained by emulsion solution blowing. Panels (a) and (b) show core–shell fibers obtained from emulsion of DCPD in PAN and DMF, while panels (c) and (d) show core–shell fibers obtained from emulsion of PAN and isophorone diisocyanate in DMF. The scale bar in all images is 10 μm.

encapsulated by the outer shell created from the 10 wt% PAN solution under the proper conditions found in this study. It is emphasized that here and hereinafter all the component concentrations in the fibers are fully determined by the initial solution concentrations and the flow rates used in the fiber forming processes. They can also be evaluated from the core and shell sizes in the images. Correspondingly, the component concentrations in dry fibers after solvent evaporation are fully predetermined by the fiber forming process and known. Once the solvent evaporated off through the shell,[34] liquid DCPD was encapsulated inside the PAN shell to form the desired core–shell PAN–DCPD nanofibers which could also be exploited for self-healing purposes in ultra-thin geometries. In addition, surface and core instabilities were occasionally observed in the collected fiber network as shown in Fig. 4b similar to Fig. 2b, which resemble capillary instabilities of liquid jets.[35] Mechanics of capillary instability of the electrified core–shell fibers has been sufficiently developed (for the review, see ref. 25 and references therein).

Fig. 2–4 show that emulsion electrospinning, emulsion solution blowing, or coelectrospinning are capable of producing core–shell fibers with healing agents encapsulated in the core. There is no doubt that the healing agents are encapsulated in the core, while polymer is in the shell because only the viscoelasticity

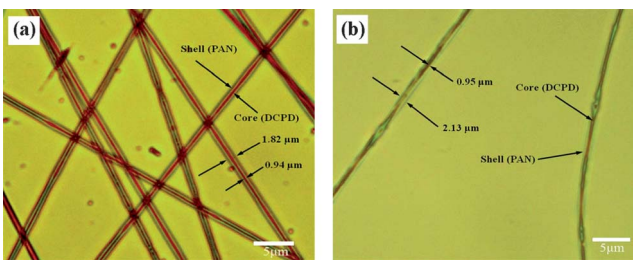

Fig. 4 Optical images of the coelectrospun core–shell PAN–DCPD nanofibers. Panels (a) and (b) illustrate different fiber morphologies. The scale bar in both images is 5 μm.

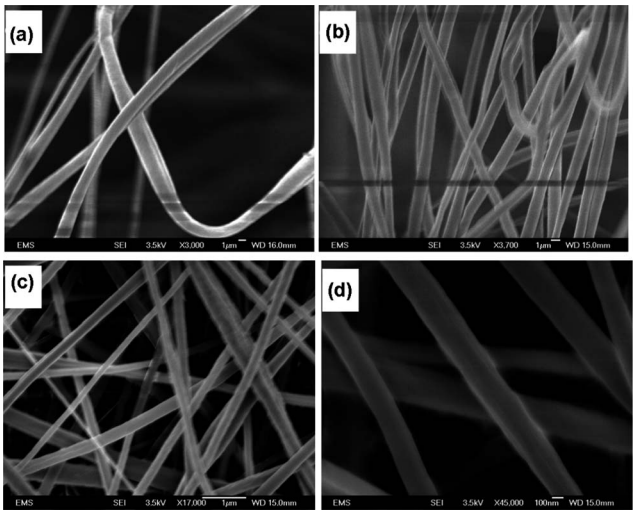

Fig. 5 SEM images of undamaged core–shell fibers. Panels (a) and (b) show isophorone diisocyanate–PAN core–shell fibers before squeezing, and panels (c) and (d) show DCPD–PAN core–shell fibers before squeezing. It can be seen that the core–shell fibers have no protrusions on their walls. The scale bars under the frames are 1 μm in (a)–(c) and 100 nm in (d).

of the polymer can provide the shell with the spinnability and structural stability needed for fiber formation.

In addition, to demonstrate the presence of the healing material in the fiber core, a fiber crush test was employed. First, the fibers were collected on a copper plate roughened by sand paper (600 grade) and the catalyst for the corresponding self-healing process was distributed on a second roughened copper plate. Then, they were pressed against each other under a mass of 1 kg overnight. In the case of isophorone diisocyanate–PAN fibers, water was used as a catalyst and for DCPD–PAN fibers tungsten(VI) chloride was chosen as a catalyst. The fibers were

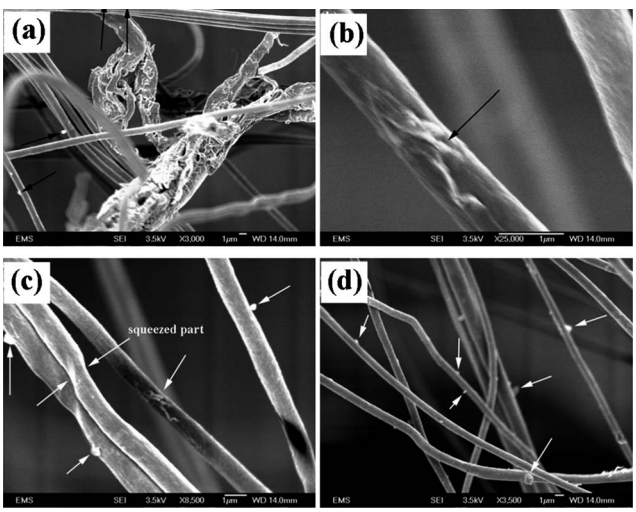

Fig. 6 SEM images of squeezed isophorone diisocyanate–PAN core–shell fibers. Panels (a)–(d) illustrate different morphological aspects. The arrows indicate solid protrusions found on the fiber walls. Under squeezing, isophorone diisocyanate is released from the fiber core, makes contact with the catalyst (water) and solidifies creating the visible protrusions. The scale bars under all frames are 1 μm.

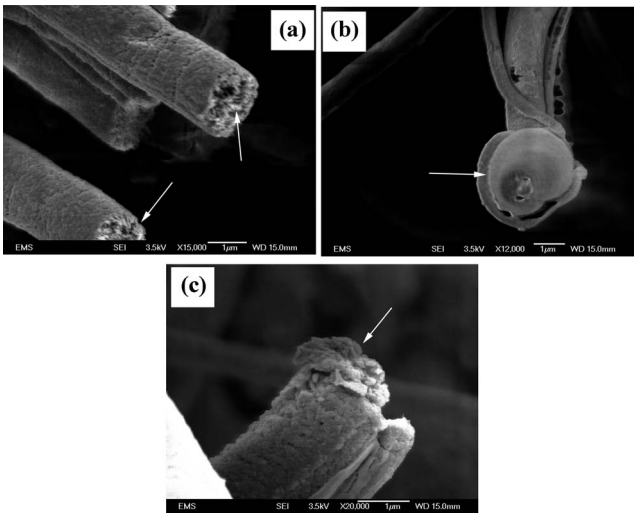

Fig. 7 SEM images of squeezed DCPD/PAN core–shell fibers. In panel (a) the arrow shows the rough cross-section of a fiber. In (b) the arrow indicates a solid blob protruding from the core and in panel (c) the arrow shows the solid protrusion formed at the end of a fiber. As a result of squeezing, DCPD is released from the fiber core, comes in contact with the catalyst [tungsten(VI) chloride] and solidifies. The scale bars under all frames are 1 μm.

observed before and after squeezing. The fibers before squeezing are shown in Fig. 5a and b (isophorone diisocyanate–PAN) and 5c and d (DCPD–PAN). The same fibers after squeezing are shown in Fig. 6 (isophorone diisocyanate–PAN) and 7 (DCPD–PAN). The fibers which were smooth before squeezing developed different protrusions at their surfaces as a result of squeezing. Namely, the fiber shell was broken at some locations and the encapsulated healing agents were released from the core. At the fiber surface, these agents came in contact with their catalysts, polymerized and solidified to form the protrusions. The release of the healing agent from the fiber core was also observed in the axial direction and the solidified blobs were formed at the fiber edges (Fig. 7).

It is also tempting to apply micro-Raman or micro-IR techniques to characterize the internal structure of core–shell fibers. However, this is impossible due to the following reasons. In micro-Raman or micro-IR techniques the spot size is of the order of 1–2 μm. To get a reliable signal from a sample, its size needs to be at least somewhat larger than the spot size. The core–shell fibers (Fig. 2–4) have the outer shell diameters of the order of 1–2 μm, and the core diameter is about 450 nm–1 μm. This clearly shows that the core diameter in most of the cases is much smaller than the spot size, which makes it impossible to receive any reliable signal from a single fiber. If it were possible to observe fiber cross-sections in a bundle of perfectly aligned core–shell fibers closely located to each other and perfectly facing the oncoming laser beam, micro-Raman or micro-IR could have shed light on the internal structure of the fibers. However, the distances between the fiber cores in the bundle would still be on the scale of 1–2 μm,[15,36] which is comparable to the spot size, which makes it impossible to obtain a reliable signal.

A number of additional experiments were conducted to prove the presence of healing materials in the fiber cores. Note first that in the present work two different self-healing core–shell structures were formed—PAN–DCPD and PAN–isophorone diisocyanate. The molecular weights of PAN, DCPD and isophorone diisocyanate are 150 kDa, 132 Da and 222 Da, respectively, and PAN is a polymer, whereas the other two compounds are monomers. Among these three compounds, only PAN possesses viscoelasticity which results in spinnability and fiber formation when PAN is in the shell, whereas DCPD or isophorone diisocyanate stays in the core, and alone would not facilitate fiber formation. The energy dispersive X-ray spectroscopy (EDX) was employed to reveal the presence of DCPD or isophorone diisocyanate in the fiber core. It is emphasized that quantification of light elements by EDX is extremely difficult and may lead to incorrect results due to absorption of low energy X-rays in a specimen, in the detector window and silicon dead layer. Also, there is an additional obstacle. To avoid any possible interference, a sample cannot be sputter-coated with metal. As a result of that, samples should be inspected in differential-pressure SEM, which employs gas ions to neutralize the electric charge. This causes the beam to widen resulting in difficulties with localization at any analysis conducted. This widening can begin from a submicron-sized spot in an ultra-high vacuum SEM to a spot of about 100 μm in differential-pressure SEM (in addition, to a possible movement of nanofiber mat under electron beam).

When energy dispersive X-ray spectroscopy (EDX) is employed, materials are characterized based on their Kα energy shell. In the core–shell nanofibers in the present work the shell consists of PAN [$(C_3H_3N)_n$] and the core is comprised of either isophorone diisocyanate ($C_{12}H_{18}N_2O_2$) or DCPD ($C_{10}H_{12}$). In PAN–DCPD core–shell system it seems that the EDX spectrum of the core (DCPD) which will show no or minimal presence of nitrogen will be easily distinguishable from the shell spectrum containing nitrogen. A careful observation of EDX series reveals that carbon corresponds to Kα value of 0.277 keV and nitrogen to 0.392 keV. The energy resolution of the detector is ~0.140 keV, which means that in the EDX spectrum positions of nitrogen and carbon overlap, which makes it impossible to perform a reliable characterization based on nitrogen presence or absence. Indeed, it can be seen from Fig. 8a and b for PAN–DCPD core–shell fibers that the N peak is, in fact, completely overshadowed by the neighboring C peak, which makes it impossible to prove the existence of DCPD in the core by EDX. On the other hand, the spectrum of cross-section of PAN–isophorone diisocyanate (Fig. 8c) is more informative. It can be seen in Fig. 8c that the oxygen peak in the core in such fibers is much higher (~8%; Fig. 8c) than that of the shell (~3%; Fig. 8a). This points out the presence of isophorone diisocyanate in the fiber core. However, the difference in the oxygen peak is not very pronounced, and the comparison of Fig. 8a and c is rather qualitative than really quantitative.

Since EDX was incapable of a reliable confirmation of the presence of DCPD in the core–shell PAN–DCPD nanofibers, we employed an indirect routine based on preferential imprinting of fluorescent dye (Rhodamine B). PAN has a melting/degradation point of 300 °C, while DCPD has a melting point of 32 °C. For the imprinting test, mats of PAN–DCPD nanofibers and of pure PAN nanofibers were cut. Then, they were immersed in a dye solution of Rhodamine B at 40 °C for two hours. After that, they were rinsed with cold water the same number of times over 24 h.

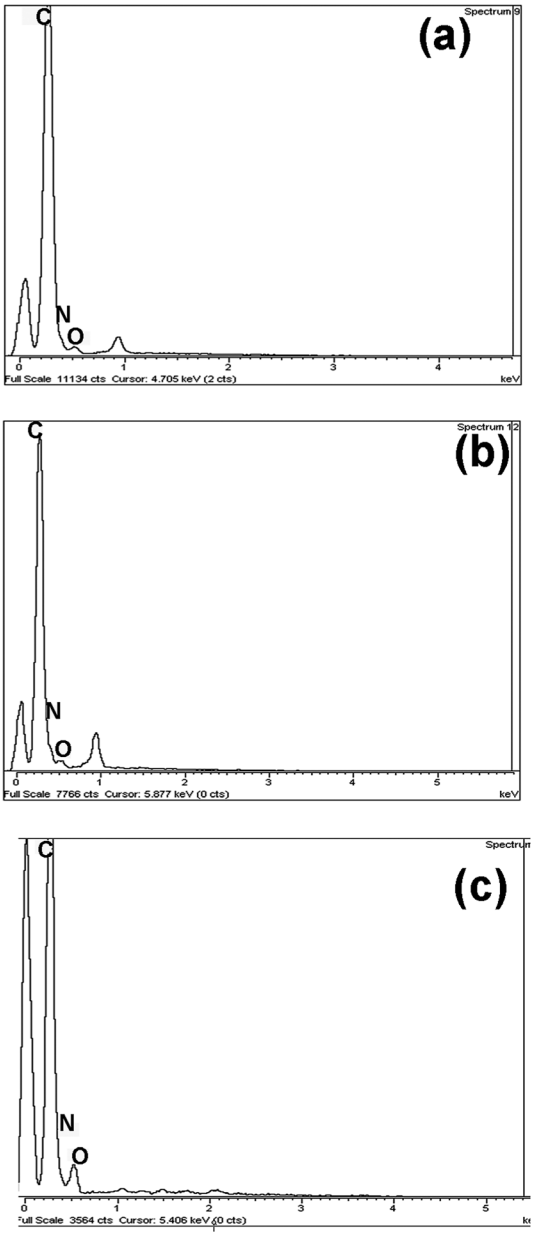

Fig. 8 EDX spectrum of (a) nanofiber shell (PAN), (b) cross-section of PAN–DCPD nanofiber. It can be seen that the presence of N is practically masked by the neighboring carbon peak in the spectrum owing to the energy resolution of the detector. Panel (c) corresponds to cross-section of PAN–isophorone diisocyanate nanofibers. Panel (c) shows a visible rise in the oxygen peak compared to panel (a). This rise is attributed to the presence of the oxygen-containing isophorone diisocyanate in the fiber core.

After the rinsing, photographs were taken of both mats for comparison (Fig. 9). In particular, Fig. 9a shows the rinsed PAN nanofiber mat, whereas Fig. 9b shows the rinsed PAN–DCPD nanofiber mat. Comparing Fig. 9a and b, one observes that the PAN–DCPD nanofiber mat in Fig. 9b is slightly pink. This can be explained as follows. For coelectrospinning, both PAN and DCPD were dissolved in the same solvent DMF. As the solvent was evaporating through the shell, pores in the shell were formed, as explained and demonstrated in ref. 34 and 28. At 40 °C DCPD

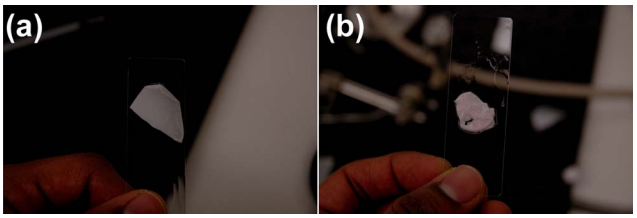

Fig. 9 (a) PAN and (b) PAN–DCPD cut nanofiber mats after the immersion in Rhodamine B solution at 40 °C with the subsequent rinsing in cold water. It can be seen that pure PAN nanofibers are white, whereas the PAN–DCPD nanofiber mat is slightly pink.

melted in the core, and the dye reached the molten core through the pores in the shell and the cut portion of the mat. The dye could adhere to molten DCPD being physically adsorbed. No strong physical adsorption is expected at 40 °C on a still solid PAN shell, or solid pure PAN fibers (Fig. 9a). Therefore, after cooling and rinsing, DCPD should still retain Rhodamine B and be pink (Fig. 9b), while rinsing of solid PAN removed all the dye and left it white. As a result, the observations in Fig. 9 show that, in the core–shell nanofibers, the core indeed contains DCPD.

In addition, to demonstrate the presence of dye adsorbed to the DCPD core, fluorescence imaging of the PAN–DCPD nanofiber mat shown in Fig. 9b was done using a Nikon microscope (Eclipse E800) equipped with a 60× objective. The optical image of the nanofiber mat is shown in Fig. 10a, whereas the fluorescent image is shown in Fig. 10b (the same place is marked by arrows in Fig. 10a and b). It can be seen that the fiber diameter is larger in Fig. 10a than in Fig. 10b. This remarkable observation stems from the fact that in Fig. 10a the fiber shell is visible, whereas in Fig. 10b only the nanofiber core is visible, which is DCPD stained by the fluorescent dye. Note that in the fluorescent image in Fig. 10b some fibers are invisible, which means that either the fluorescent dye did not reach the core through the pores in those sections or it was rinsed even from the core there during the subsequent rinsing. The observations in Fig. 10 conclusively prove the presence of DCPD in the fiber core.

The CNT samples intercalated with the healing agents were inspected under the TEM (Fig. 11) and compared to a CNT image before the intercalation used for control (Fig. 12). Fig. 11a and b show DCPD intercalated into CNTs, and Fig. 11c and d show isophorone diisocyanate intercalated into CNTs. Both figures demonstrate that the CNT bores were filled with the healing agents. Furthermore, the outside of the CNTs is clean of any deposits, which reveals that the rinsing process was

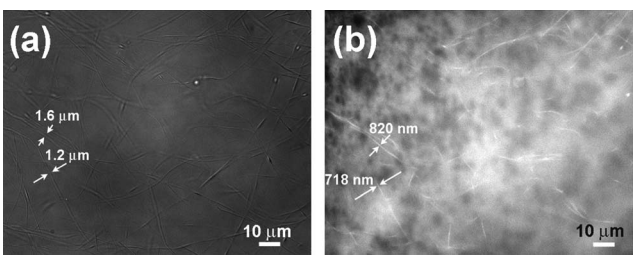

Fig. 10 (a) Optical image and (b) fluorescent image of the fiber mat shown in Fig. 9b.

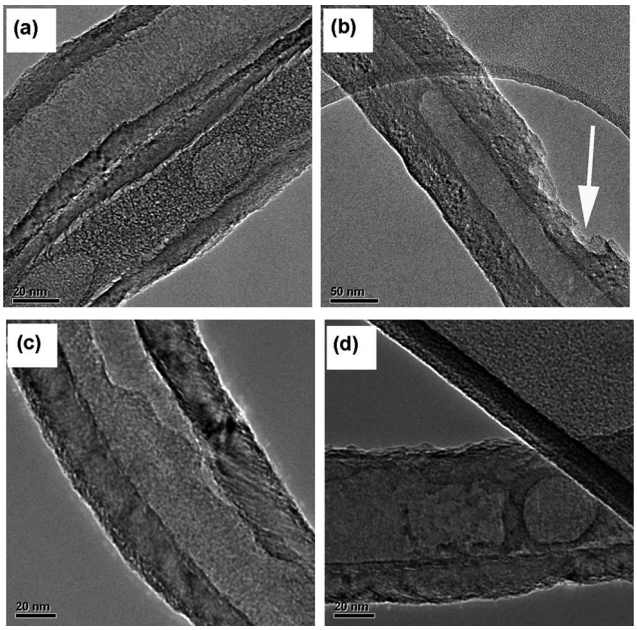

Fig. 11 TEM images of the intercalated self-healing materials inside CNTs. Panels (a) and (b) show DCPD inside CNTs, while (c) and (d) show isophorone diisocyanate inside CNTs. In panel (b) the arrow indicates the partially broken CNT wall.

sufficiently effective. In Fig. 11b one can see that the CNT wall was partially broken by the sonication; the broken location is marked by the arrow. This observation shows that the amorphous turbostratic CNTs used in the present work can be easily broken, which facilitates release of the healing agents. It is emphasized that all the TEM images in Fig. 11 were captured over the holes in the holey carbon grid, which allowed us to avoid the contrast associated with the carbon film used for support.

Fig. 13 shows a typical failed surface of self-healing composite samples after interlaminar fracture. It can be observed that the core–shell PAN nanofibers were well entangled with the epoxy resin at the interface to form an ultrathin self-healing nanofiber-reinforced nanocomposite layer between neighboring

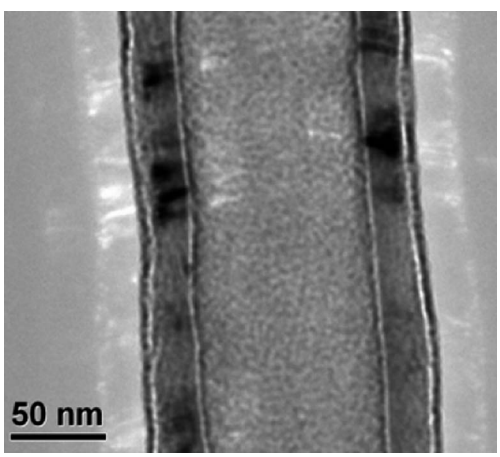

Fig. 12 TEM image of an empty CNT before the intercalation of self-healing materials.

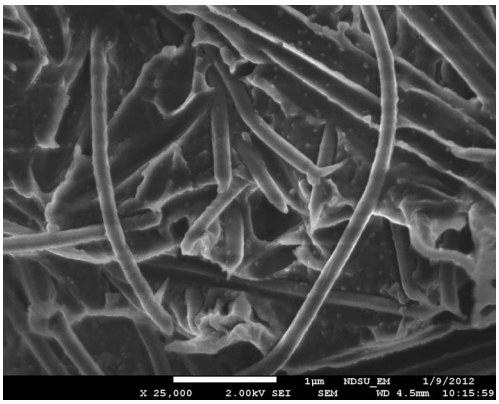

Fig. 13 SEM image of core–shell PAN nanofiber-toughened interface.

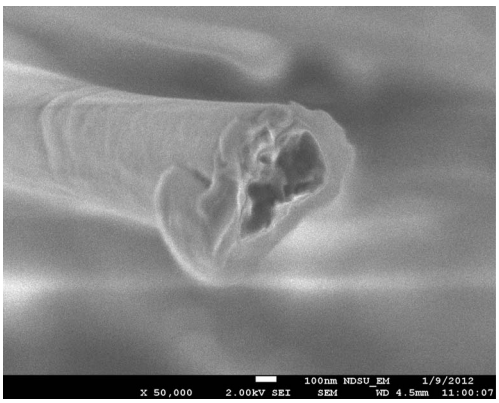

Fig. 14 SEM image of a failed core–shell PAN nanofiber at the interface with depleted healing agent.

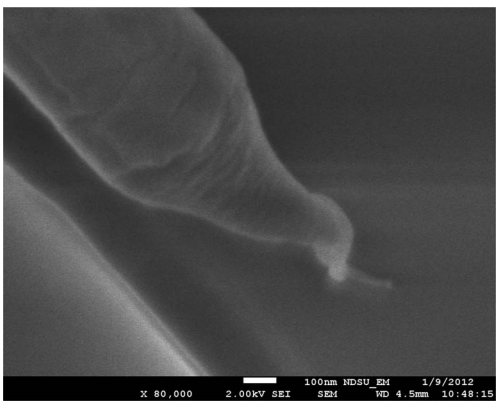

Fig. 15 SEM image of a failed core–shell PAN nanofiber at the interface with released healing agent.

carbon-fiber fabrics. The failure (toughening) modes include nanofiber pull-out, debonding, breakage, plastic necking, matrix cracking and related stress shielding and crack kinking in the matrix interlayers, similar to those induced by solid electrospun PAN nanofibers as studied previously.[20] These failure modes are expected to dissipate significant strain energy compared to pure resin failure (cracking) in virgin polymer composite without nanofiber reinforcement at the interface. Furthermore, once

nanofibers broke, liquid DCPD was released under the action of the external stressing and capillary effect as shown in Fig. 13–15. In particular, Fig. 14 shows a failed core–shell structure with an empty core region due to release of the healing agent, while Fig. 15 shows the conic structure due to the release (pull-out) of liquid (soft) healing agent. If touched with catalyst particles dissolved in a composite matrix, ring-opening polymerization would be triggered and heal the interfacial crack as expected. Thus, the present SEM-based fractographical analysis has explored the main toughening mechanisms at composite interfaces and also validated the deliverability of self-healing agent at composite interfaces.

4. Conclusion

Emulsion electrospinning, emulsion solution blowing, and coelectrospinning of core–shell fibers using PAN as the fiber-forming shell have been successfully applied to encapsulate healing agents, such as DCPD or isophorone diisocyanate, in the fiber core. The core–shell structure of the fibers was observed visually by using an optical microscope. In addition, the presence of the healing agents in the core was demonstrated in the fiber crush tests. Namely, when the fibers were squeezed between two copper plates in the presence of their corresponding catalysts the healing agents were released through the broken fiber shell or at the broken fiber cross-sections. After the release, the healing agents polymerized and solidified to form multiple protrusions which were observed through SEM. The presence of the healing materials in the fiber core was also revealed by energy dispersive X-ray spectroscopy, and preferential imprinting of a fluorescent dye.

The intercalation of the healing agents into amorphous turbostratic carbon nanotubes by means of the self-sustained diffusion method was also successfully demonstrated. Furthermore, it was also observed that such carbon nanotubes can be relatively easily broken which facilitates release of healing agents.

Finally, novel proof-of-concept hybrid polymer composites reinforced with self-healing core–shell nanofibers at the interfaces have been produced, and relevant toughening mechanisms and deliverability of healing agent examined and validated. All of the preceding techniques provide a plethora of ways to encapsulate healing materials to be used in production of smart composites with embedded self-healing agents on a mass scale.

Acknowledgements

The authors are grateful to Yiyun Zhang for constructive discussion regarding fluorescent microscopy, Dr Alan Nicholls for his help with electron microscopy and Dr Michael Cho for the access to his fluorescent microscope.

References

1 E. B. Murphy and F. Wudl, *Prog. Polym. Sci.*, 2010, **35**, 223.
2 C. B. Bucknall, I. C. Drinkwater and G. R. Smith, *Polym. Eng. Sci.*, 1980, **20**, 432.
3 J. P. Youngblood and N. R. Sottos, *MRS Bull.*, 2008, **33**, 732.
4 S. R. White, N. R. Sottos, P. H. Geubelle, J. S. Moore, M. R. Kessler, S. R. Sriram, E. N. Brown and S. Viswanathan, *Nature*, 2001, **409**, 794.
5 R. P. Wool, *Nature*, 2001, **409**, 773.
6 S. M. Bleay, C. B. Loader, V. J. Hawyes, L. Humberstone and P. T. Curtis, *Composites, Part A*, 2001, **32**, 1767.
7 B. J. Blaiszik, N. R. Sottos and S. R. White, *Compos. Sci. Technol.*, 2008, **68**, 978.
8 S. van der Zwaag, *Self-healing Materials: An Alternative Approach to 20 Centuries of Materials Science*, Springer, Dordrecht, 2007.
9 K. S. Toohey, N. R. Sottos, J. A. Lewis, J. S. Moore and S. R. White, *Nat. Mater.*, 2007, **6**, 581.
10 R. M. Jones, *Mechanics of Composite Materials*, Taylor & Francis, Philadelphia, 2nd edn, 1999.
11 Y. A. Dzenis and D. H. Reneker, *US Pat.*, 6265333, 2001.
12 Y. Dzenis, *Science*, 2008, **319**, 419.
13 J. Doshi and D. H. Reneker, *J. Electrost.*, 1995, **35**, 151.
14 D. H. Reneker and I. Chun, *Nanotechnology*, 1996, **7**, 216.
15 D. H. Reneker, A. L. Yarin, E. Zussman and H. Xu, *Adv. Appl. Mech.*, 2007, **41**, 43.
16 D. H. Reneker and A. L. Yarin, *Polymer*, 2008, **49**, 2387.
17 Y. Dzenis, *Science*, 2004, **304**, 1917.
18 Z. Sun, E. Zussman, A. L. Yarin, J. H. Wendorff and A. Greiner, *Adv. Mater.*, 2003, **15**, 1929.
19 E. Zussman, A. L. Yarin, A. V. Bazilevsky, R. Avrahami and M. Feldman, *Adv. Mater.*, 2006, **18**, 348.
20 X. Wu, *Fracture of Advanced Composites with Nanostructured Interfaces: Fabrication, Characterization and Modeling*, VDM Verlag, Germany, 2009.
21 S. Lin, Q. Cai, J. Y. Ji, G. Sui, Y. H. Yu, X. P. Yang, Q. Ma, Y. Wei and X. L. Deng, *Compos. Sci. Technol.*, 2008, **68**, 3322.
22 E. Ozden, Y. Z. Menceloglu and M. Papila, *ACS Appl. Mater. Interfaces*, 2010, **2**, 1788.
23 Q. Chen, L. F. Zhang, A. Rahman, Z. P. Zhou, X. F. Wu and H. Fong, *Composites, Part A*, 2011, **42**, 2036.
24 A. L. Yarin, E. Zussman, J. H. Wendorff and A. Greiner, *J. Mater. Chem.*, 2007, **17**, 2585.
25 A. L. Yarin, *Polym. Adv. Technol.*, 2011, **22**, 310.
26 A. L. Yarin, S. Koombhongse and D. H. Reneker, *J. Appl. Phys.*, 2001, **90**, 4836.
27 A. V. Bazilevsky, A. L. Yarin and C. M. Megaridis, *Langmuir*, 2007, **23**, 2311.
28 S. Sinha-Ray, Y. Zhang, A. L. Yarin, S. C. Davis and B. Pourdeyhimi, *Biomacromolecules*, 2011, **12**, 2357.
29 S. Sinha-Ray, A. L. Yarin and B. Pourdeyhimi, *Carbon*, 2010, **48**, 3575.
30 D. H. Reneker, A. L. Yarin, H. Fong and S. Koombhongse, *J. Appl. Phys.*, 2000, **87**, 4531.
31 A. V. Bazilevsky, K. Sun, A. L. Yarin and C. M. Megaridis, *Langmuir*, 2007, **23**, 7451.
32 A. V. Bazilevsky, K. Sun, A. L. Yarin and C. M. Megaridis, *J. Mater. Chem.*, 2008, **18**, 696.
33 S. Sinha-Ray, R. P. Sahu and A. L. Yarin, *Soft Matter*, 2011, **7**, 8823.
34 Y. Dror, W. Salalha, R. Avrahami, E. Zussman, A. L. Yarin, R. Dersch, A. Greiner and J. H. Wendorff, *Small*, 2007, **3**, 1064.
35 A. L. Yarin, *Free Liquid Jets and Films: Hydrodynamics and Rheology*, Longman Scientific & Technical and Wiley & Sons, New York, 1993.
36 A. Theron, E. Zussman and A. L. Yarin, *Nanotechnology*, 2001, **12**, 384.

